Available online at www.sciencedirect.com

ScienceDirect

journal homepage: www.elsevier.com/locate/he

Mechanical milled doped Zn-based semiconductors powders for photovoltaic devices

J.I. Laborde [a], J. Hoya [a], M.D. Reyes Tolosa [b], M.A. Hernandez-Fenollosa [b], L.C. Damonte [a,c,*]

[a] Departamento de Física, Facultad de Ciencias Exactas, Universidad Nacional de La Plata (UNLP), CC 67, 1900 La Plata, Argentina

[b] Instituto de Tecnología de Materiales, Universitat Politècnica de València, 46022 Camino de Vera s/n, Valencia, Spain

[c] Instituto de Física La Plata (IFLP, CONICET), La Plata, Argentina

ARTICLE INFO

Article history:
Received 21 October 2013
Accepted 5 December 2013
Available online 4 February 2014

Keywords:
Nanocrystalline semiconductors
Mechanical milling
Photovoltaic cells

ABSTRACT

Structural characterization of nanocrystalline Al-doped ZnTe semiconductors, obtained by mechanical milling from ZnTe and Al_2O_3 powders, is presented. The samples were analyzed by X-ray diffraction (XRD), scanning electron microscopy (SEM), X-ray absorption full spectroscopy (XAFS) and positron annihilation lifetime (PALS) measurements. The results suggested that Al atoms are substitutional incorporated into the ZnTe cubic structure.

1. Introduction

Among II–VI semiconductors zinc telluride (ZnTe) is very attractive for optoelectronic device applications in the green spectral range, due to its direct wide band gap (~2.26 eV) [1–3]. It usually has a cubic crystal structure; it is a material of high absorption coefficient and shows p-type characteristics. Since zinc telluride can be easily doped and being a low cost semiconductor material, it can be used as different constituent for solar cells, for example, as a back-surface field layer and p-type semiconductor material for a CdTe/ZnTe structure [3–5] or as the inorganic element in hybrid solar cells. ZnTe alloys have been obtained with different morphologies and using a variety of methods such as electrodeposition [6], pulsed laser deposition (PLD) [7], thermal evaporation [8,9], molecular beam epitaxy (MBE), magnetron sputtering [10] and mechanical alloying techniques [11,12].

Mechanical alloying (MA) is a room temperature solid-state route able of synthesizing a variety of equilibrium and non-equilibrium alloys, including nanocrystalline phases and amorphous compounds [13,14]. This technique in addition to its versatility has many advantages, like low cost, easy control of composition and large scale production.

It is known that solar cells efficiency may be improved increasing charge carriers densities and interfacial processes. New kind of materials, different assemblies, etc has been studied during the last decades. In particular, the development of nanomaterials production has opened a great amount

* *Corresponding author*. Instituto de Física La Plata (IFLP, CONICET), 1900 La Plata, Argentina.
E-mail addresses: mareto@upvnet.upv.es (M.D. Reyes Tolosa), mhernan@upvnet.upv.es (M.A. Hernandez-Fenollosa), damonte@fisica.unlp.edu.ar, lcdamonte@gmail.com (L.C. Damonte).

0360-3199/$ – see front matter
http://dx.doi.org/10.1016/j.ijhydene.2013.12.051

of research in this area. In this sense, our goal is investigate nanopowders and nanocolumns, prepared by low cost methods [15,16] and its doping with donor elements. In previous works we have successfully obtained ZnO nanopowders and nanocolumns doped with Al and In and analyzed their structural and optical properties [16,17].

Recently, other II–VI semiconductor as ZnTe and ZnSe were subjected to mechanical work and their structural characteristic were studied by means of X-ray diffraction and positron annihilation measurements.

In this work, we concentrate in the Al doping of ZnTe by mechanical milling and its structural characterization. Nanosized doped powders were analyzed by X-ray diffraction, X-ray Absorption Full Spectroscopy (XAFS), scanning electron microscopy (SEM) and positron annihilation lifetime (PALS) measurements. The results, compared with undoped powders, will allow us to improve the performance of hybrid organic/inorganic solar cells.

2. Experimental procedure

Stoichiometric quantities were weighed to obtain mixtures of ZnTe (99.99% from Aldrich Chemistry) with 5 at% Al_2O_3 (99.9%), powders provided by Alfa Aesar Johnson Matthey Co. The powders were milled in a steel cylinder (8 cm^3) with one steel ball (diameter 12 mm) in air atmosphere being the ball mass to powder mass ratio of 10/1. The mechanical milling was performed in a Retsch MM2 horizontal vibratory mill at a frequency of 30 Hz during different milling times (1, 5 and 10 h).

Starting and milled powders were characterized by X-Ray diffraction (XRD) performed with a Philips PW1710 Diffractometer with CuKα radiation in the National Diffraction Laboratory (LANADI-UNLP).

Powder microstructure was also investigated by scanning electron microscopy (SEM) with a JSM–6300 (JEOL Scanning Microscopy) operating at 10 kV in the UPV (Valencia – Spain).

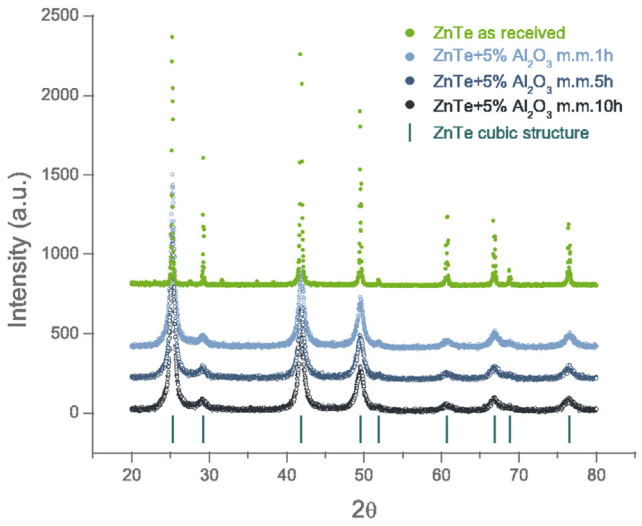

Fig. 1 – X-ray diffractograms for pure and doped ZnTe, at different milling times.

X-ray Absorption Full Spectroscopy (XAFS) measurements were taken at room temperature in transmission mode at the Zn K-edge, using a Si(111) monochromator at the XAFS1 beam line of LNLS (Campinas, Brazil).

Milled powders were then compacted under uniaxial pressure of 150 MPa into disk-shaped pellets (diameter 8 mm).

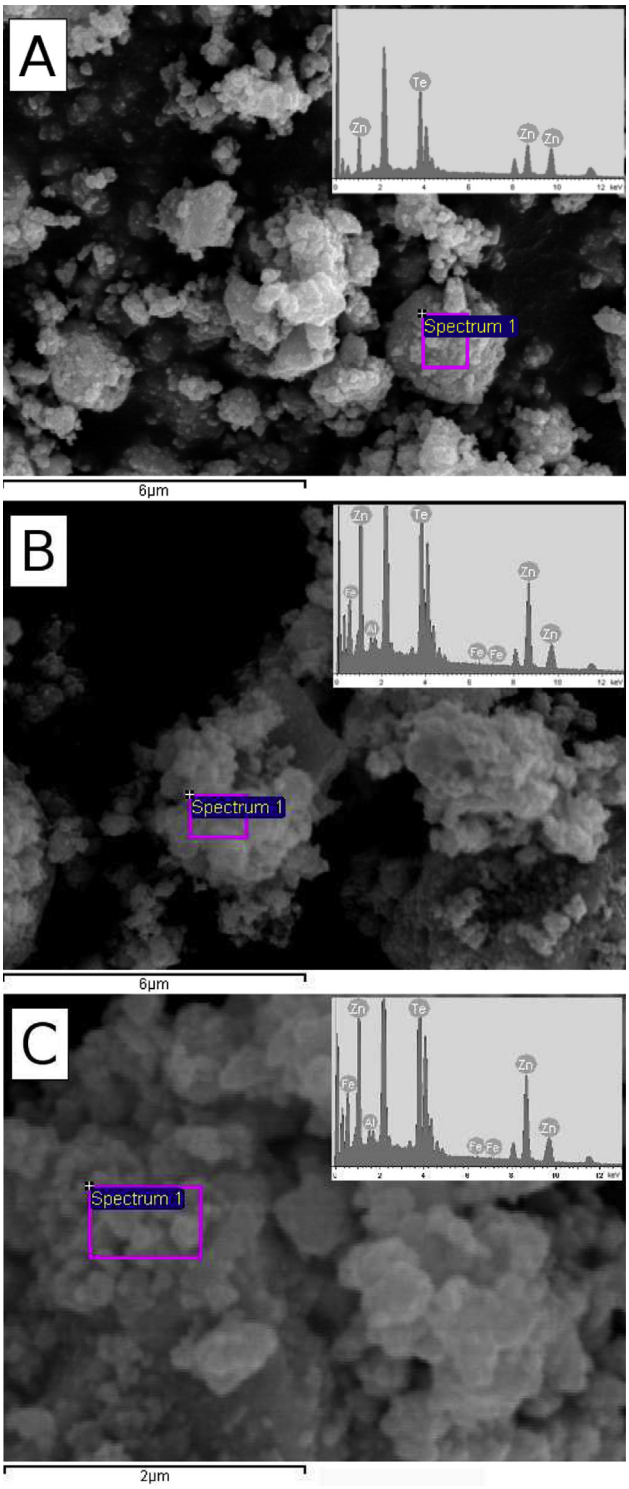

Fig. 2 – SEM micrographs for: A) pure ZnTe after 10 h of milling; B) and C) Al-doped ZnTe after 1 and 10 h of milling. Insent show EDS analysis at the signed region.

Positron Annihilation Lifetime measurements (PALS) were done in a conventional fast–fast coincidence system with two scintillator detectors (one BaF_2 and one plastic BURLE) provided a time resolution (FWHM) of 260 ps. A $^{22}NaCl$ (10 μCi) radioactive source deposited onto a kapton foil (1.42 g/cm^3) and sandwiched between two identical samples was used. The source contribution and the response function were evaluated from a Hf metal reference sample using the RESOLUTION code [18]. Positron lifetime spectra of 3×10^6 counts each were recorded at room temperature and analyzed with the POSITRONFIT program [18].

3. Results and discussion

The XRD patterns for the ZnTe powders, as received and milled 1, 5 and 10 h with 5 at% Al_2O_3, are shown in Fig. 1. For all of them, the diffractograms display the reflection lines of cubic (F43m) ZnTe, with a peak broadening, consequence of grain size reduction [19]. For doped samples no additional peaks are observed, even for those samples after low milling times where a low contribution from Al_2O_3 is expected.

Fig. 2 shows SEM micrographs for pure and Al-doped ZnTe after milling. The inset displays EDS analysis result at the indicated site. As milling proceeds, grain size diminution and agglomeration are observed. In Al-doped samples, the presence of Fe atoms, evidenced from EDS analysis, indicate iron contamination from milling tools. The Fe atomic % increases with milling time from 0.19 to 0.59, while for pure ZnTe no contamination is observed even after 10 h of milling. This low content of Fe was not reported in the X-ray analysis.

In order to get information on doping atom incorporation into the host semiconductor some XAFS analysis were done. Fig. 3 shows the XAFS function χ(R) for Al-doped ZnTe as function of milling time. For comparison undoped ZnTe is also shown. The results were analyzed using the IFFEFIT software, with the Athena implementation. In a very preliminary way, we conclude that the distance from Zn to nearest neighbours do not change, neither with milling time nor with the addition of dopants. There is a diminution in the principal peak amplitude in all cases with respect the starting material. Also, both, milling and doping processes have a little effect at low values of R to the left of the main peak.

Fitting procedure was carried out using the FEFF7 phase and amplitudes. The ATOMS code was used as a tool to generate the input files for FEFF7 based on the ZnTe crystallography data. The Fourier Transformed (FT) EXAFS data of ZnTe starting sample is shown in Fig. 4. If TeO_2 is include not significant improvement is observed. Instead, for milled pure and doped ZnTe the inclusion of zinc and telluride oxide, improve the fits at low values of R. We take into account only the first coordination sphere of both oxides that corresponds to Zn–O and Te–O distances. Although this incorporation, they have relatively low amplitudes. Moreover, we try the inclusion of Al_2O_3 or Al metal in order to analyze the incorporation of the dopant atom into the ZnTe structure but the final fit was not better. The results are shown in Fig. 5.

The lifetime spectra for all samples consist in various exponential decays

$$n(t) = \sum_i I_i \exp(-t/\tau_i)$$

being the relative intensities I_i, normalized, $S_i = 1$. After background subtraction, and convolution with the resolution function, the parameters that characterized each positron state, λ_i annihilation rate ($\lambda_i = 1/\sigma_i$) and its intensity I_i, are obtained by means of POSITRONFIT program [18]. The PALS spectra were decomposed into two exponential decays, assuming a source correction with two components, one of 386 ps of 15% intensity assigned to kapton foil and a second one of around 1 ns with less than 1% intensity due to annihilation in the surroundings of the source. The presence of two lifetime components is an usual feature for II–VI semiconductors compounds, since intrinsic and extrinsic defects introduced during crystal growth and doping are unavoidable [20]. Also mechanical milling introduces a certain amount of defects such as vacancies, interstitials, etc [13]. All these point defects constitute positron trapping centers leading to similar positron lifetime components unable to be separate. So we have evaluated the average positron lifetime defined by

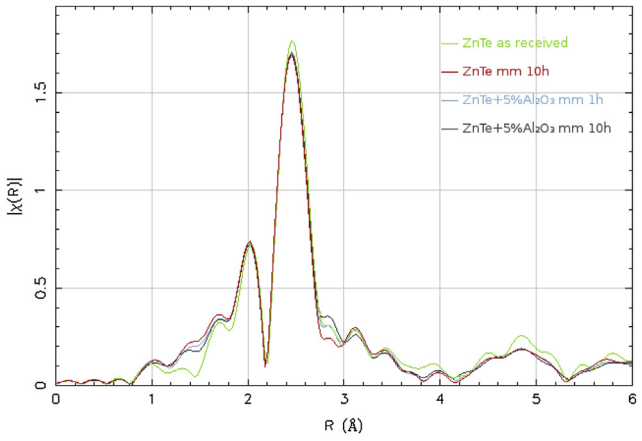

Fig. 3 – XAFS function for pure and doped ZnTe as milling time increases.

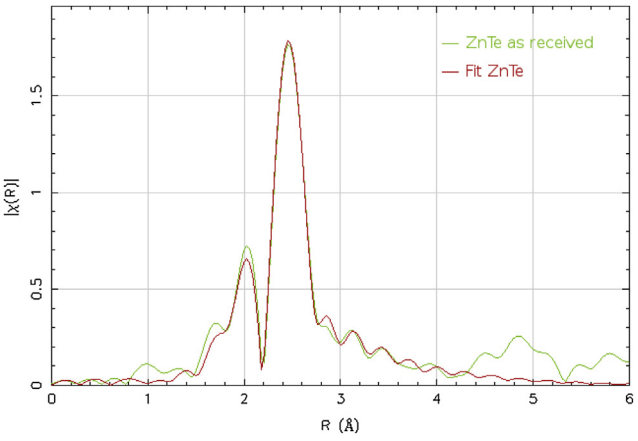

Fig. 4 – χ(R) for pure ZnTe, red line represent the result of the fit. (For interpretation of the references to color in this figure legend, the reader is referred to the web version of this article.)

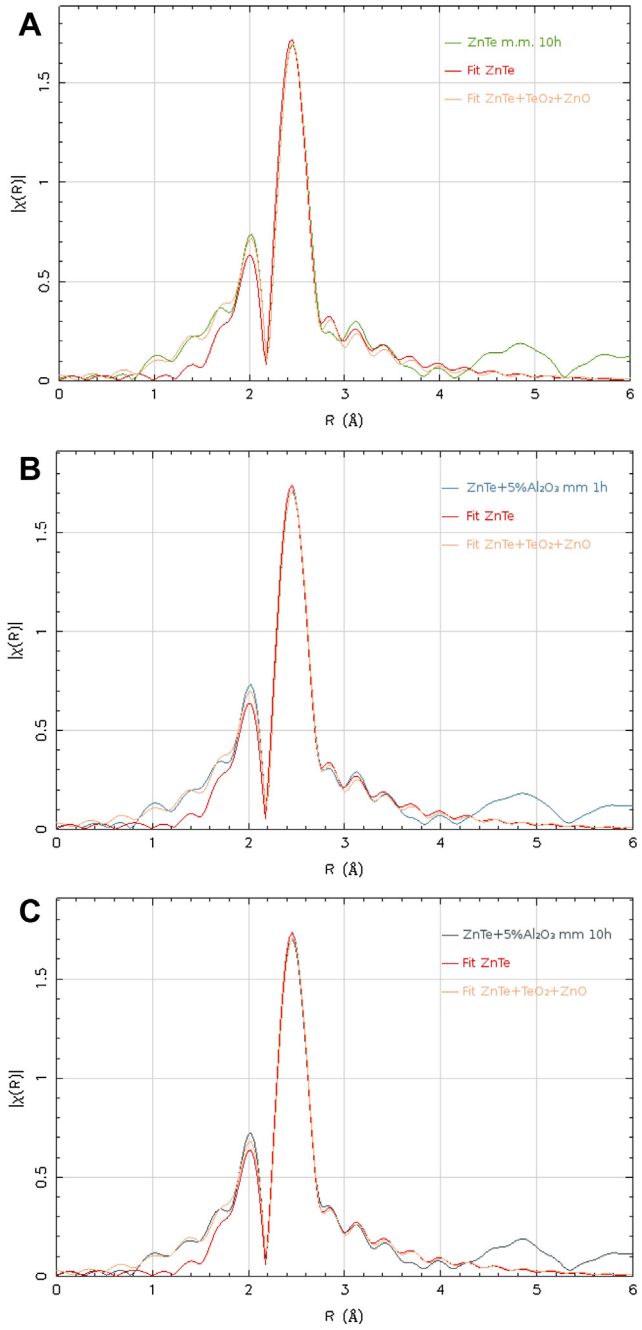

Fig. 5 – χ(R) data together with fitting results: A) pure ZnTe, B) Al-doped ZnTe after 1 h of milling, C) Al-doped ZnTe after 1° h of milling. Orange lines represent the result of the fit including the oxides. (For interpretation of the references to colour in this figure legend, the reader is referred to the web verson of this article.)

$$\tau_{ave} = \sum_i I_i \tau_i$$

a useful parameter almost independent of data treatment. From this statistical parameter, one can extract information about the evolution of positron traps.

The resulting values for pure and doped zinc telluride are summarized in Table 1.

Table 1 – Average positron lifetime for pure and Al-doped ZnTe.

Sample	Milling time (h)	τ_{ave}(ps)
ZnTe	0	321
	10	342
Al–ZnTe	0	351
	5	353
	10	357

It can be seen that the values for Al-doped ZnTe are similar to the pure and milled compound. As was already conclude for doped ZnO [16], this fact can be interpreted as an incorporation of doping atom into the semiconductor structure since no other lifetime contribution is observed.

4. Conclusions

It is proved that mechanical milling is a simple, cheap and effective method to obtain nanocrystalline aluminum doped zinc telluride powders from ZnTe and Al_2O_3 mixtures. From X-ray diffraction and SEM images the nanocrystalline nature of the powders is confirm. Also, no trace is observed of other compounds than ZnTe. XAFS measurements gave information of a kind of surface oxidation since the results admit a small contribution of ZnO and TeO_2. In addition, since no aluminum compound can be included in the analysis they also give evidence of aluminum incorporation into the ZnTe crystalline structure. Moreover, positron annihilation lifetime spectroscopy became an effective tool to sense dopant incorporation into ZnTe power through the average lifetime evolution with milling time. However, a slight iron contamination from milling tools is observed from EDS analysis for the doped samples.

Optical characterization is now in course in order to give support to dopant incorporation into the semiconductor structure and its effect on the specific properties towards their photovoltaic applications.

Acknowledgments

This work was supported by the CONICET (PIP 112-200802-00128) from Argentina. Authors also acknowledge Dr. Marcos Meyer for his collaboration.

REFERENCES

[1] Kvit A, Oktyabrsky S. Defects in CdTe and related compounds encyclopedia of materials: science and technology. 2nd ed.; 2001. pp. 1985–9.
[2] Hakan Gürel H, Ünlü Hilmi. Density functional and tight binding theories of electronic properties of II–VI heterostructures. Mat Sci Semicond Process 2013;16:1619–28.
[3] Gilic M, Romcevic N, Romcevic M, Stojanovic D, Kostic R, Trajic J, et al. Optical properties of CdTe/ZnTe self-assembled quantum dots: Raman and photoluminescence spectroscopy. J Alloys Compd 2013;579:330–5.

[4] Feng X, Singh K, .Bhavanam S, Palekis V, Morel D-L, Ferekides C. Preparation and characterization of ZnTe as an interlayer for CdS/CdTe substrate thin film solar cells on flexible substrates. Thin Solid Films 2013;535:202–5.
[5] Kozlovsky VI, Krysa AB, V Korostelin Yu, .G Sadofyev Yu. MBE growth and characterization of ZnTe epilayers and ZnCdTe/ZnTe structures on GaAs(1 0 0) and ZnTe(1 0 0) substrates. J Crystal Growth 2000;214–215:35–9.
[6] Jiang Y, Kou H, Li J, Yu S, Du Y, Ye W, et al. Synthesis of ZnTe dendrites on multi-walled carbon nanotubes/polyimide nanocomposite membrane by electrochemical atomic layer deposition and photoelectrical property research. J Solid State Chem 2012;194:336–42.
[7] Ghosh B, Ghosh D, Hussain S, Bhar R, Pal AK. Growth of ZnTe films by pulsed laser deposition technique. J Alloys Compd 2012;541:104–10.
[8] Ko H, Park S, An S, Lee C. Intense near-infrared emission from undoped ZnTe nanostructures synthesized by thermal evaporation. J Alloys Compd 2013;580-15:316–20.
[9] Güllü HH, Bayraklı Ö, Candan İ, Coşkun E, Parlak M. Structural and optical properties of Zn–In–Te thin films deposited by thermal evaporation technique. J Alloys Compd 2013;566:83–9.
[10] Zhang Z, Li J, Zhang H, Pan X, Xie E. Thickness-dependent field emission from ZnTe films prepared by magnetron sputtering. J Alloys Compd 2013;549:88–91.
[11] Hoya J, Laborde JI, Damonte LC. Structural characterization of mechanical milled ZnSe and ZnTe powders for photovoltaic devices. Int J Hydrogen Energy 2012;37:14769–72.
[12] Patra S, Pradhan SK. Quickest single-step one pot mechanosynthesis and characterization of ZnTe quantum dots. J Alloys Compd 2011;509:5567–70.
[13] Suryanarayana C. Mechanical alloying and milling. Progr Mater Sci 2001;46(1):184.
[14] Damonte LC, Mendoza-Zélis LA, Deledda S, Eckert J. Effect of preparation conditions on the short-range order in Zr-based bulk glass-forming alloys. Mat Sc and Eng 2003;A343:194–8.
[15] Damonte LC, Donderis V, Ferrari S, Meyer M, Orozco J, Hernández Fenollosa MA. ZnO-based nanocrystalline powders with applications in hybrid photovoltaic cells. Int Journal of Hydrogen Energy 2010;35:5834–7.
[16] Reyes Tolosa MD, Orozco-Messana J, Damonte LC, Hernandez-Fenollosa MA. ZnO nanoestructured layers processing with morphology control by pulsed electrodeposition. J Electrochem Soc 2011;158:D452–5.
[17] Damonte LC, Donderis V, Hernández Fenollosa MA. Trivalent dopants on ZnO semiconductor obtained by mechanical milling. J Alloys Compd 2009;483(1–2):442–84.
[18] Kirkegaard P, Pedersen NJ, Eldrup M. PATFIT-88 Riso-M-2740; 1989. Risø.
[19] Damonte LC, Mendoza Zélis LA, Marí Soucase B, Hernández Fenollosa MA. Nanoparticles of ZnO obtained by mechanical milling. Powder Technol 2004;148:1519.
[20] Krause-Rehberg R, Leipner HS, Abgarjan T, Polity A. Review of defect investigations by means of positron annihilation in II-VI compound semiconductors. Appl Phys A 1998;66:599–614.